

ALTA-TH-12-03

ANL-HEP-PR-03-100

See-Saw Induced CMSSM Lepton-Flavour Violation Post-WMAP

Bruce A. Campbell¹ David W. Maybury¹ and Brandon Murakami²

¹*Department of Physics, University of Alberta, Edmonton AB T6G 2J1, CANADA*

²*High Energy Physics Division, Argonne National Laboratory, Argonne, IL 60439 USA*

Abstract

The see-saw mechanism of neutrino mass generation, when incorporated in supersymmetric theories with supergravity mediated supersymmetry breaking, results in low-energy lepton-flavour violation arising from the soft supersymmetry breaking slepton masses. The parameter space of supergravity theories with conserved R -parity is severely constrained by the requirement that the LSP provide cold dark matter with a relic density in the range indicated by the recent WMAP measurements, as well as by laboratory constraints. We calculate the $\mu \rightarrow e\gamma$ branching ratio for the constrained minimal supersymmetric standard model, over the range of parameters consistent with WMAP and laboratory constraints, in families of see-saw model parameterizations which fit the low energy neutrino measurements. We find that over much of the range of see-saw models, for supersymmetry parameters consistent with WMAP and laboratory bounds, the resulting predicted rates for $\mu \rightarrow e\gamma$ (and other charged lepton flavour violating processes) are within current experimental limits, but that these rates should be detectable with the next generation of lepton-flavour violation experiments.

1 Introduction

The standard model contains three continuous global symmetries associated with lepton flavour. Neglecting non-perturbative effects arising from the weak $SU(2)$ anomaly, the standard model conserves lepton flavour exactly, as the charged Yukawa matrix \mathbf{Y}_e and the gauge interactions can simultaneously be made flavour diagonal. The solar [1]–[5], and atmospheric [6], neutrino deficit observations, which imply neutrino mass and mixing, (and their confirmation by reactor [7], and accelerator [8], experiments), presently provide the only direct observation of physics that cannot be accommodated within the standard model. The smallness of the inferred neutrino masses can be understood through the see-saw mechanism [9], which involves the introduction of a heavy Majorana fermion in a gauge singlet (right-handed neutrino) for each generation. The light neutrino masses are then induced through a Yukawa interaction of the form $N_i^c \mathbf{Y}_\nu^{ij} L_j H$, once the right-handed neutrinos are integrated out at the Majorana scale, M_R . The resulting induced neutrino mass operator arises at dimension 5 ($HHLL$) and, on dimensional grounds, would be expected to be the first observable extension beyond the renormalizable dimension 4 operators that compose the standard model interactions, given the standard model particle content at low energies.

Even without the addition of a see-saw sector generating neutrino masses, the standard model suffers from a gauge hierarchy problem, with quadratic divergences in radiative corrections to the Higgs mass parameter. These require unnatural fine-tuning of the input Higgs parameters, readjusted at each order in perturbation theory, in order to maintain the hierarchy of scales between the gravitational energy scale M_{Pl} , and the scale of electroweak breaking M_W . A natural solution to this problem is the supersymmetric extension of the standard model, where the extra particles and interactions necessitated by supersymmetry contribute cancelling contributions to the destabilizing quadratic divergences in the Higgs potential, as required by the supersymmetry non-renormalization theorems. After soft supersymmetry breaking the cancellation of the quadratic divergences will still remain, though there will be finite shifts of the Higgs mass parameters by an amount proportional to the soft supersymmetry breaking. Model dependence enters in the choice of mechanism to impose the

soft supersymmetry breaking. An especially attractive and well-motivated possibility is that the supersymmetry breaking is communicated (super-)gravitationally from a hidden sector in which supersymmetry is spontaneously broken, to the observable sector of the supersymmetric standard model (mSUGRA). Models with soft supersymmetry breaking masses of the form that this mechanism would impose, and where each of the soft supersymmetry breaking scalar masses, gaugino masses and trilinear couplings are universal and flavour diagonal at the Planck scale, comprise the constrained minimal supersymmetric standard model (CMSSM).

To incorporate see-saw neutrino masses in a supersymmetric extension of the standard model, we consider the minimal supersymmetric standard model with additional right-handed (singlet) neutrino supermultiplets and their superpotential interactions, where each of the soft supersymmetry breaking scalar masses, gaugino masses and trilinear couplings are universal and flavour diagonal at the Planck scale. New indirect sources of low-energy lepton-flavour violation (LFV) appear with the introduction of the singlet neutrino supermultiplets. Renormalization group running of the slepton mass matrices and trilinear couplings in the presence of right-handed neutrinos generates off diagonal elements that contribute to LFV processes [10],

$$(\Delta m_L^2)_{ij} \approx -\frac{1}{8\pi^2}(3+a^2)m_0^2(\mathbf{Y}_\nu^\dagger \mathbf{Y}_\nu) \ln\left(\frac{M_{GUT}}{M_R}\right) \quad (1)$$

where M_R is the Majorana scale. As the see-saw mechanism violates lepton number by two units, the CMSSM with right-handed neutrino singlets continues to conserve R -parity; therefore the lightest supersymmetric particle (LSP) is stable. If it is assumed that the dark matter is composed of the LSP (which is expected to be the lightest neutralino), the CMSSM parameter space becomes tightly constrained by the WMAP satellite observations [11], as well as by laboratory searches. These constraints [12, 13, 14] have important implications for the rates of lepton-flavour violating processes.

In this study, we examine CMSSM lepton-flavour violation [15, 16] in simple general classes [17] of see-saw models which are constructed to fit the low energy neutrino oscillation data. The parametrization of see-saw models is considered in Section 2. Two specific classes

[17] of them (corresponding to hierarchical or degenerate Majorana masses for the singlet right-handed neutrinos) form the model range of our calculations in Section 4. The models considered have their neutrino Yukawa couplings (and Majorana mass scale) chosen as large as reasonable, to maximize the rates for lepton-flavour violating decays; this is a conservative assumption, as we wish to consider how much of CMSSM parameter space (and see-saw model space) is still consistent with experimental limits on lepton-flavour violation, and this is conservatively determined under assumptions that maximize its calculated rate.

In Section 3 we discuss the range of parameter space of the CMSSM over which we perform our calculations. The CMSSM parameters are chosen such that their renormalization group running to low energies yields radiative electroweak symmetry breaking, and a resulting spectrum of particle masses that is consistent with experiment. In particular, we display our results over CMSSM parameter ranges determined by [12] and [13], which impose that the resulting models have LSP relic densities in the region determined by WMAP [11], and are consistent with the LEP direct search limits, and the rate for $b \rightarrow s\gamma$. See also [14] for other parameter determinations using WMAP and laboratory data.

In Section 4 we compute the branching ratio for the decay $\mu \rightarrow e\gamma$ [15, 16], in the classes of see-saw models considered, over the allowed range of CMSSM parameter space, and compare to present [19], and prospective [20], data for this process. We consider $\mu \rightarrow e\gamma$ because with the present level of experimental precision, lepton-flavour violation in the models and parameter ranges we consider would only be detectable in muon decays. Of the muon decays, since the rates for $\mu \rightarrow eee$, and $\mu N \rightarrow eN$, are largely dominated by electromagnetic penguin contributions (again, in the models and parameter ranges we consider), they are suppressed with respect to the rate for $\mu \rightarrow e\gamma$ by an extra factor of α . Since at the present time the experimental limit on $\text{BR}(\mu \rightarrow e\gamma) \leq 1.2 \times 10^{-11}$ [19], is of comparable strength to the limits on $\text{BR}(\mu \rightarrow eee) \leq 1.0 \times 10^{-12}$ [21], and $\text{BR}(\mu N \rightarrow eN) \leq 6.1 \times 10^{-13}$ [22], the model class that we study will be consistent with all the present lepton-flavour violation data if it satisfies the present limit on $\text{BR}(\mu \rightarrow e\gamma)$. We will find that even for a choice of neutrino Yukawa coupling (and Majorana scale) that maximizes the rates for lepton-flavour violation,

that much of the model space and parameter range is consistent with present experimental limits, though future experiments should probe these ranges thoroughly, at least for the largest choices of Yukawa couplings.

In Section 5 we present our conclusions. For a thorough review of muon physics and muon flavour violation, see [25].

2 Supersymmetric see-saw Parameterization

The leptonic part of the CMSSM see-saw superpotential is

$$\mathcal{L} = \mathbf{Y}_e^{ij} \epsilon_{\alpha\beta} H_d^\alpha e_i^c L_j^\beta + \mathbf{Y}_\nu^{ij} \epsilon_{\alpha\beta} H_u^\alpha N_i^c L_j^\beta + \frac{1}{2} \mathcal{M}^{ij} N_i^c N_j^c \quad (2)$$

above the Majorana scale. Here, L_i , $i = e, \mu, \tau$, is the left handed weak doublet, e_i^c is the charged lepton weak singlet, and H_u and H_d are the two Higgs doublets of opposite hypercharge. The anti-symmetric SU(2) tensor is defined by $\epsilon_{12} = +1$. N denotes the right-handed neutrino singlet. The Yukawa matrices \mathbf{Y}_e and \mathbf{Y}_ν give masses to the charged leptons and Dirac masses to the neutrinos respectively. The Majorana matrix, \mathcal{M}^{ij} , gives the right-handed neutrinos their heavy Majorana mass. Below the Majorana scale the right-handed neutrinos are integrated out, and after renormalization down to the scale of electroweak symmetry breaking, induce a Majorana mass for the light left-handed neutrinos via the see-saw mechanism,

$$\mathbf{m}_\nu = \mathbf{Y}_\nu^T \mathcal{M}^{-1} \mathbf{Y}_\nu < H_u^0 >^2 \quad (3)$$

where $< H_u^0 >^2 = v_2^2 = v^2 \sin^2 \beta$ and $v = (174 \text{ GeV})^2$ as set by the Fermi constant G_F . By transforming to a basis where \mathbf{Y}_e and the gauge interactions are flavour diagonal, the left-handed neutrino mass matrix is diagonalized by the MNS matrix \mathbf{U} ,

$$\mathbf{U}^T \mathbf{m}_\nu \mathbf{U} = \text{diag}(m_1, m_2, m_3) \quad (4)$$

where \mathbf{U} is a unitary matrix that connects flavour states to the mass eigenbasis. It is possible to parameterize the MNS matrix as follows,

$$\mathbf{U} = \mathbf{U}' \text{diag}(e^{-i\phi/2}, e^{-i\phi'}, 1) \quad (5)$$

$$\mathbf{U}' = \begin{pmatrix} c_{13}c_{12} & c_{13}s_{12} & s_{13}e^{-i\delta} \\ -c_{23}s_{12} - s_{23}s_{13}c_{12}e^{i\delta} & c_{23}c_{12} - s_{23}s_{13}s_{12}e^{i\delta} & s_{23}c_{13} \\ s_{23}s_{12} - c_{23}s_{13}c_{12}e^{i\delta} & -s_{23}c_{12} - c_{23}s_{13}s_{12}e^{i\delta} & c_{23}c_{13} \end{pmatrix}. \quad (6)$$

where ϕ and ϕ' are additional CP violating phases and \mathbf{U}' has the usual form of the CKM matrix. It was shown in [17] that the Yukawa matrix Y_ν can be re-expressed in a simple general form. By defining,

$$\kappa \equiv \frac{\mathbf{m}_\nu}{\langle H_u^0 \rangle^2} = \mathbf{Y}_\nu^T \mathcal{M}^{-1} \mathbf{Y}_\nu \quad (7)$$

and using the MNS matrix, it is possible to diagonalize κ ,

$$\kappa_d = \mathbf{U}^T \mathbf{Y}_\nu^T \mathcal{M}^{-1} \mathbf{Y}_\nu \mathbf{U}. \quad (8)$$

where the d subscript denotes diagonalization. It is always possible to make an arbitrary field re-definition to rotate to a basis such that \mathcal{M} is diagonal, hence $\mathcal{M}_d = \text{diag}(\mathcal{M}_1, \mathcal{M}_2 \mathcal{M}_3)$.

In this case,

$$\mathbf{1} = \left(\sqrt{\mathcal{M}_d^{-1}} \mathbf{Y}_\nu \mathbf{U} \sqrt{\kappa_d^{-1}} \right)^T \left(\sqrt{\mathcal{M}_d^{-1}} \mathbf{Y}_\nu \mathbf{U} \sqrt{\kappa_d^{-1}} \right) \quad (9)$$

where a square root over a diagonal matrix denotes the positive square root of its entries.

One then identifies

$$\mathbf{R} \equiv \sqrt{\mathcal{M}_d^{-1}} \mathbf{Y}_\nu \mathbf{U} \sqrt{\kappa_d^{-1}} \quad (10)$$

as an arbitrary orthogonal matrix. Then, the most general form of \mathbf{Y}_ν is [17]

$$\mathbf{Y}_\nu = \sqrt{\mathcal{M}_d} \mathbf{R} \sqrt{\kappa_d} \mathbf{U}^\dagger. \quad (11)$$

As pointed out by the authors of [17], the physical low-energy observables contained in \mathbf{U} and κ_d are augmented by three positive mass eigenvalues associated with \mathcal{M} and three (in general complex) parameters that define the orthogonal matrix \mathbf{R} . It should be stressed that the above equation is defined at the Majorana scale, M_R . It is useful to parameterize the neutrino Yukawa couplings with the use of an arbitrary orthogonal matrix, \mathbf{R} , as it allows a general examination of the origin of flavour violation in see-saw models.

Following [17] we will consider two classes of neutrino hierarchy models. In the first case we will examine a strong right-handed neutrino hierarchy and in the second, we will consider

degenerate right-handed neutrinos. In both cases we will assume that the Yukawa couplings of the left-handed neutrinos are hierarchical. We will impose the condition that the largest eigenvalue of the $\mathbf{Y}_\nu^\dagger \mathbf{Y}_\nu$ matrix (denoted $|Y_0|^2$) coincide with the square of the top quark Yukawa coupling $|Y_t|^2$ at the unification scale M_{GUT} . This Yukawa unification condition is suggested in simple $SO(10)$ models, and has the effect of making the neutrino Yukawa couplings, and hence the rates for lepton-flavour violating processes, as large as reasonably possible. Since we are interested in the degree to which present experimental limits rule out regions of model and CMSSM parameter space, maximizing the expected rates gives us a conservative determination of the models and parameter ranges that are still viable. More specific details of the classes of models to be analyzed will be discussed in Section 4.

3 Supersymmetry Breaking and the CMSSM

Since supersymmetric particles have not yet been observed, the model Lagrangian must contain terms that break supersymmetry. If we assume that supersymmetry is broken softly, in that the supersymmetry violating terms are of mass dimension 2 and 3, then the Lagrangian has the following supersymmetry breaking terms,

$$\begin{aligned}
-\mathcal{L}_{\text{soft}} = & (\mathbf{m}_{\tilde{\mathbf{L}}}^2)_{ij} \tilde{L}_i^\dagger \tilde{L}_j + (\mathbf{m}_{\tilde{\mathbf{e}}}^2)_{ij} \tilde{e}_{Ri}^* \tilde{e}_{jR} + (\mathbf{m}_{\tilde{\nu}}^2)_{ij} \tilde{\nu}_{Ri}^* \tilde{\nu}_{Rj} \\
& + (\mathbf{m}_{\tilde{\mathbf{Q}}}^2)_{ij} \tilde{Q}_i^\dagger \tilde{Q}_j + (\mathbf{m}_{\tilde{\mathbf{u}}}^2)_{ij} \tilde{u}_{Ri}^* \tilde{u}_{jR} + (\mathbf{m}_{\tilde{\mathbf{d}}}^2)_{ij} \tilde{d}_{Ri}^* \tilde{d}_{jR} \\
& + \tilde{m}_{H_d}^2 H_d^\dagger H_d + \tilde{m}_{H_u}^2 H_u^\dagger H_u + (B\mu H_d H_u + \frac{1}{2} B_\nu \mathcal{M}_{ij} \tilde{\nu}_{Ri}^* \tilde{\nu}_{Rj}^* + \text{h.c.}) \\
& [(\mathbf{A}_{\tilde{\mathbf{d}}})_{ij} H_d \tilde{d}_{Ri}^* \tilde{Q}_j + (\mathbf{A}_{\tilde{\mathbf{u}}})_{ij} H_u \tilde{u}_{Ri}^* \tilde{Q}_j + (\mathbf{A}_{\tilde{\mathbf{l}}})_{ij} H_d \tilde{e}_{Ri}^* \tilde{L}_j + (\mathbf{A}_\nu)_{ij} H_u \tilde{\nu}_{Ri}^* L_j \\
& + \frac{1}{2} M_1 \tilde{B}_L^0 \tilde{B}_L^0 + \frac{1}{2} M_2 \tilde{W}_L^a \tilde{W}_L^a + \frac{1}{2} M_3 \tilde{G}^a \tilde{G}^a + \text{h.c.}]
\end{aligned} \tag{12}$$

Note the presence of terms containing $\mathbf{m}_{\tilde{\nu}}^2$ and \mathbf{A}_ν in eq.(12). These terms are only included above the Majorana scale. Below the Majorana scale, the soft part of the Lagrangian returns to that of the CMSSM. In the CMSSM scenario, supersymmetry is broken in a universal *i.e.*, flavour independent, manner giving the following relations

$$(\mathbf{m}_{\tilde{f}}^2)_{ij} = m_0^2 \mathbf{1} \quad \tilde{m}_{h_i}^2 = m_0^2 \quad \mathbf{A}_{fij} = a m_0 \mathbf{Y}_f, \tag{13}$$

where m_0 is a universal scalar mass and a is a dimensionless constant. We restrict to the CMSSM in our studies and set the trilinear A-term soft parameter $a = 0$. The ranges for the other non-zero, Planck-scale, inputs to the CMSSM are chosen such that their renormalization group running to low energies yields radiative electroweak symmetry breaking, and a resulting spectrum of particle masses that is consistent with experiment. In particular, we display our results over CMSSM parameter ranges determined by [12] and [13], which not only impose that the resulting model have LSP relic densities in the range determined by WMAP [11], but that they have spectra consistent with the LEP direct search limits, as well as the rate for $b \rightarrow s\gamma$. Following these authors we ignore the focus point region in parameter space which occurs at very large m_0 and whose location depends on m_t and M_H in an extremely sensitive manner.

Note that the absence of off-diagonal terms leads to flavour conservation (up to effects of light neutrino mass splittings). However, these relations are imposed at the GUT scale and are therefore subject to renormalization group running. Above the Majorana scale, the neutrino sector modifies the CMSSM renormalization group equations (RGEs). In fact, the flavour violation is controlled by the off-diagonal terms in $\mathbf{Y}_\nu^\dagger \mathbf{Y}_\nu$, which contribute to the off-diagonal terms of $\mathbf{m}_{\tilde{L}}^2$. In the leading log approximation to the RGEs we have,

$$\begin{aligned} (\mathbf{m}_{\tilde{L}}^2)_{ij} &\approx -\frac{1}{8\pi^2}(3+a^2)m_0^2(\mathbf{Y}_\nu^\dagger \mathbf{Y}_\nu)_{ij} \ln \frac{M_{GUT}}{M_R} \\ (\mathbf{m}_{\tilde{e}}^2)_{ij} &\approx 0 \\ (\mathbf{A}_e)_{ij} &\approx -\frac{3}{8\pi^2}am_0\mathbf{Y}_e(\mathbf{Y}_\nu^\dagger \mathbf{Y}_\nu)_{ij} \ln \frac{M_{GUT}}{M_R} \end{aligned} \quad (14)$$

It is the presence of such terms that leads to significant flavour violation. We will see in the following sections how much flavour violation we should expect, and how the branching ratio for the process $\mu \rightarrow e\gamma$ is affected. The branching ratio for $\mu \rightarrow e\gamma$ can be estimated through mass insertion techniques [15, 16]:

$$\begin{aligned} \text{BR}(\mu \rightarrow e\gamma) &\sim \frac{\alpha^3}{G_F^2} \frac{(\mathbf{m}_{\tilde{L}ij})^2}{m_s^8} \tan^2 \beta \\ &\sim \frac{\alpha^3}{G_F^2 m_s^8} \left| \frac{-1}{8\pi^2}(3+a^2)m_0^2 \ln \frac{M_{GUT}}{M_R} \right|^2 \left| (\mathbf{Y}_\nu^\dagger \mathbf{Y}_\nu)_{ij} \right|^2 \tan^2 \beta \end{aligned} \quad (15)$$

where m_s is a typical slepton mass. We note that the branching ratio is proportional to $\tan^2 \beta$, which will give an increasing dependence on the ratio of Higgs vevs $\tan \beta$, and will be evident in our detailed results in the next section.

4 $\mu \rightarrow e\gamma$ In The CMSSM See-Saw

Following [17] we consider two classes of neutrino hierarchy models. In both cases the neutrino Yukawa couplings to the left-handed neutrinos are assumed to be hierarchical. In the first class of models the Majorana mass terms for the singlet right-handed see-saw neutrinos are assumed to be strongly hierarchical. In the second, we will assume that the right-handed singlet neutrinos have degenerate Majorana masses. We numerically integrate the one loop CMSSM RGEs with right-handed neutrino supermultiplets. In addition, we have re-derived the expressions [15] for the amplitude for $\mu \rightarrow e\gamma$, and we use the resulting full expressions (see Appendix) to calculate the branching ratios.

4.1 Hierarchical ν_R s

As we saw in Section 2, \mathbf{Y}_ν can be expressed using an orthogonal matrix, \mathbf{R} . Following [17], and ignoring possible phases, it is useful to parameterize \mathbf{R} as,

$$\mathbf{R} = \begin{pmatrix} c_2 c_3 & -c_1 s_3 - s_1 s_2 c_3 & s_1 s_3 - c_1 s_2 c_3 \\ c_2 s_3 & c_1 c_3 - s_1 s_2 s_3 & -s_1 c_3 - c_1 s_2 s_3 \\ s_2 & s_1 c_2 & c_1 c_2 \end{pmatrix}. \quad (16)$$

Since we are assuming that the left-handed neutrinos are hierarchical, we take

$$\kappa_2 = \sqrt{\frac{(\Delta m_\nu^2)_{\text{sol}}}{v_2^4}} \quad \kappa_3 = \sqrt{\frac{(\Delta m_\nu^2)_{\text{atm}}}{v_2^4}}, \quad (17)$$

and based on the bi-maximal LMA mixing solution we take the MNS matrix to be,

$$\mathbf{U}_{\text{MNS}} \approx \begin{pmatrix} .866 & .500 & 0 \\ -.354 & .612 & .707 \\ .354 & -.612 & .707 \end{pmatrix}. \quad (18)$$

If we assume a strong hierarchy in the right-handed sector, then

$$(\mathbf{Y}_\nu)_{ij} = \sqrt{\mathcal{M}_3} \delta_{i3} \mathbf{R}_{3l} (\sqrt{\kappa_d})_l \mathbf{U}_{lj}^\dagger. \quad (19)$$

The largest eigenvalue of eq.(19) is $Y_0 = \mathcal{M}_3 (|\mathbf{R}_{32}|^2 \kappa_2 + |\mathbf{R}_{33}|^2 \kappa_3)$. We identify this with the top coupling at M_{GUT} as in the case of many $SO(10)$ models. By identifying the largest Yukawa in the neutrino sector with the top coupling LFV is maximized. We assume that $\mathbf{R}_{32} \neq 0$ or $\mathbf{R}_{33} \neq 0$. The pathology of the case where $\mathbf{R}_{32} = 0$ or $\mathbf{R}_{33} = 0$ is discussed in [17], which forms a small region of parameter space. With these assumptions, $M_R \sim 10^{15}$ GeV. This leaves us with one complex parameter. Following [17], we will assume that this parameter is real. Therefore, \mathbf{Y}_ν will depend on one angle, denoted by θ_1 in eq.(16).

First, consider figure 1. This plot shows $BR(\mu \rightarrow e\gamma)$ as a function of θ_1 and is made with parameters typical of the WMAP regions of [12], as indicated in the caption. The angle θ_1 varies over 0 to π and we only show the $\mu > 0$ case as the plots with $\mu < 0$ are very similar. Most of θ_1 is allowed for low to moderate $\tan \beta \lesssim 40$. Notice that there are two special places where the branching ratio becomes highly suppressed. These choices for θ_1 correspond to the vanishing of the off diagonal element $(\mathbf{Y}_\nu^\dagger \mathbf{Y}_\nu)_{12}$ which results in large flavour suppression. The special angles are,

$$\tan \theta_1 \approx -\sqrt{\frac{\kappa_3}{\kappa_2}} \frac{\mathbf{U}_{13}^*}{\mathbf{U}_{12}^*} \approx 0 \quad \tan \theta_1 \approx -\sqrt{\frac{\kappa_3}{\kappa_2}} \frac{\mathbf{U}_{23}^*}{\mathbf{U}_{22}^*}. \quad (20)$$

In order to quantify and further illustrate the regions that are both LFV and CMSSM compliant in this scenario, consider figures 2 and 3. The regions considered are a parameterization of the WMAP data from [12]. In figure 2, the bands correspond to $\tan \beta = 5, 10, 15, 20, 25, 30, 35, 40, 45, 50, 55$ for $\mu > 0$ and each colour represents the percentage of the θ_1 range that is allowed by the current bound on $\mu \rightarrow e\gamma$, $BR(\mu \rightarrow e\gamma) < 1.2 \times 10^{-11}$. Grey indicates that less than 25% of θ_1 is allowed, while red, green and blue illustrate that between 25% and 50%, 50% and 75%, and between 75% and 100% is allowed respectively. Notice that there are two competing effects controlling the amount of LFV in these plots. As we move higher in $\tan \beta$, the branching ratio, $BR(\mu \rightarrow e\gamma)$ increases as eq.(15). At the same time, the rate becomes suppressed at larger m_0 and $m_{1/2}$. As figure 2 illustrates, there

are portions of the parameter space at high $\tan\beta$, (*i.e.* $\gtrsim 45$), that are consistent with the current LFV bound due to the high universal scalar and gaugino mass in those regions. Figure 3 shows the situation after a possible null result from MEG, $(\text{BR}(\mu \rightarrow e\gamma) \lesssim 5 \times 10^{-14})$. We see that a large portion of the parameter space would be highly restricted, with most of the parameter space relegated to less than 25%. Therefore, the θ_1 range will be thoroughly probed by the up coming experiments, given this see-saw scenario. In the $\mu < 0$ case, the situation is slightly different. While the branching ratio of $\mu \rightarrow e\gamma$ is largely insensitive to the sign of μ , the WMAP compliant parameter space is not [13]. Figure 4 shows the constraints from lepton flavour violation with the current limit on $\text{BR}(\mu \rightarrow e\gamma) < 1.2 \times 10^{-11}$ over the WMAP range for $\mu < 0$ and $a = 0$ with $\tan\beta = 10, 35$. Grey indicates that less than 25% of θ_1 is allowed, while red, green and blue illustrate that between 25% and 50%, 50% and 75%, and between 75% and 100% is allowed respectively. The funnel structure in figure 4 for $\mu < 0$ appears at lower $\tan\beta$ (*i.e.* ~ 35) compared to figure 2. This pushes the parameter space to larger values of m_0 and $m_{1/2}$ at lower $\tan\beta$ and therefore allows more room where the WMAP region is LFV compliant. Figure 5 shows how figure 4 changes after the expected results from MEG. If LFV is not observed in the near future, this scenario will only allow a small region of θ_1 corresponding to values near those given in eq.(20) with $\mu > 0$, or a relatively moderate region of θ_1 with $\mu < 0$.

4.2 Degenerate ν_R s

Ignoring possible phases in \mathbf{R} , lepton-flavour violation becomes \mathbf{R} -independent, in the case of degenerate singlet right-handed neutrino Majorana masses. We see from eq.(11) that, $\mathbf{Y}_\nu \mathbf{Y}_\nu^\dagger$, which controls the amount of lepton flavour violation becomes

$$\mathbf{Y}_\nu^\dagger \mathbf{Y}_\nu = \mathcal{M} \mathbf{U} \kappa_d \mathbf{U}^\dagger, \quad (21)$$

which is independent of \mathbf{R} . Again, we use the GUT relation $|Y_0| \sim \mathcal{M} \kappa_3 = |Y_t(M_{\text{GUT}})|$ as in [17]. The situation here is quite different from the hierarchical case. Figure 6 shows the currently allowed region for $\mu \rightarrow e\gamma$ consistent with the CMSSM for $\mu > 0$ [12]. Notice that most of the parameter space is ruled out in this scenario; only $\tan\beta \lesssim 5$ and a small region

at $\tan \beta \approx 50$ are consistent with the current LFV bounds. The upcoming limits will probe all of this currently allowed region. In the $\mu < 0$ [13] case more of the parameter space is allowed as the region is pushed to higher soft mass scales and therefore the LFV rates become suppressed as before. Figure 7 illustrates the allowed region consistent with the current LFV bounds for $\mu < 0$. Clearly the degenerate case, with maximized “unification” neutrino Yukawa couplings, is strongly constrained by the present data and will be severely probed by the forth-coming generation of experiments.

5 Conclusion

In this paper, we examined CMSSM lepton-flavour violation in simple general classes of see-saw models [17] which had been constructed to fit the data on low energy neutrino oscillations. The models considered have had their neutrino Yukawa couplings (and Majorana mass scale) chosen as large as reasonable, to maximize the rates for lepton-flavour violating decays. Nevertheless, when the CMSSM parameters for the models were restricted (following [12, 13]) to have LSP relic densities in the region determined by WMAP, and to be consistent with the LEP direct search limits, and the rate for $b \rightarrow s\gamma$, the resulting rate for lepton-flavour violation was such that over much of the allowed WMAP range, much of the model parameter space was consistent with the present experimental limit on $\text{BR}(\mu \rightarrow e\gamma)$ (and so, a fortiori, with present limits on the other (charged) lepton-flavour violating processes). We also noted that the next generation of $\mu \rightarrow e\gamma$ experiments should definitively probe the range of branching ratios suggested by these models at maximal Yukawa couplings, and also for ranges of smaller Yukawas depending on the CMSSM parameters and the exact see-saw model details.

A future detection of $\mu \rightarrow e\gamma$ would, however, represent not the end of lepton-flavour violation studies of these models, but rather just the beginning. To disentangle the details of CMSSM see-saw lepton flavour violation will require comparisons of rates for different LFV muon decays, including $\mu \rightarrow eee$, and $\mu N \rightarrow eN$. It will also require the observation of (charged) lepton-flavour violation in different generations, such as $\tau \rightarrow \mu\gamma$, $\tau \rightarrow e\gamma$, $\tau \rightarrow \mu ll$,

and $\tau \rightarrow ell$, with l either e or μ . With a combination of observed rates for different LFV μ -decays, and the observation of LFV in τ decays, one can hope to begin to uncover both the precise nature of the low-energy soft supersymmetry breaking, as well as the origin of the lepton-flavour violating interactions responsible for inducing these decays. Fortunately, we can look forward to a new generation of dedicated $\mu \rightarrow e\gamma$ [20], and $\mu N \rightarrow eN$ [23],[24] experiments, as well as to τ sources of unprecedented flux, to help us find the experimental signatures of this new realm of physics.

6 Acknowledgements

We are deeply indebted to the authors of [12], and [13], for permission to use their figures for the WMAP and laboratory allowed regions of CMSSM parameter space, on which we have overlayed our results for the lepton-flavour violation rates. We especially thank Keith Olive for guidance on the inputs into the determinations of the allowed regions shown in different publications. We would also like to thank Carlos Wagner and Ernest Jankowski for helpful discussions. BC and DM acknowledge the support of the Natural Sciences and Engineering Research Council of Canada. BM was supported by the U.S. Department of Energy under contract W-31-109-Eng-38.

References

- [1] R. Davis, [Homestake Collaboration] Rev.Mod.Phys.75:985-994(2003).
- [2] J.N. Abdurashitov et al., [SAGE Collaboration]
 Phys.Lett.B328:234-248(1994), [arXiv:astro-ph/9907131].
 Phys.Rev.Lett.83:4686-4689(1999), [arXiv:astro-ph/9907131].
 J.Exp.Theor.Phys.95:181-193(2002), [arXiv:astro-ph/0204245].
- [3] P. Anselmann et al., [GALLEX Collaboration]
 Phys.Lett.B285:390-397(1992).

Phys.Lett.B357:237-247(1995), Erratum-ibid.B361:235-236(1996).
 Phys.Lett.B447:127-133(1999).
 Phys.Lett.B490:16-26(2000), [arXiv:hep-ex/0006034].

[4] S. Fukuda et al., [Super-Kamiokande Collaboration]
 Phys.Rev.Lett.86:5651-5655(2001), [arXiv:hep-ex/0103032].
 Phys.Rev.Lett.86:5656-5660(2001), [hep-ex/0103033].

[5] Q.R. Ahmad et al., [SNO Collaboration]
 Phys.Rev.Lett.87:071301(2001), [arXiv:nucl-ex/0106015].
 Phys.Rev.Lett.89:011301(2002), [nucl-ex/0204008].
 Phys.Rev.Lett.89:011302(2002), [nucl-ex/0204009].
 submitted for publication [nucl-ex/0309004].

[6] Y. Fukuda et al., [Super-Kamiokande Collaboration]
 Phys.Rev.Lett.81:1562-1567(1998), [arXiv:hep-ex/9807003].
 Phys.Rev.Lett.82:2644-2648(1999), [hep-ex/9812014].
 Phys.Rev.Lett.85:3999-4003(2000), [hep-ex/0009001].

[7] K. Eguchi et al., [KAMLAND Collaboration]
 Phys.Rev.Lett.90:021802(2003), [arXiv:hep-ex/0212021].

[8] M.H. Ahn et al., [K2K Collaboration]
 Phys.Rev.Lett.90:041801(2003), [arXiv:hep-ex/0212007].

[9] For reviews see:
Journeys Beyond The Standard Model
 P. Ramond, Perseus Books (1999)
Physics of Neutrinos
 M. Fukugita and T. Yanagida, Springer-Verlag (2003)

[10] F. Borzumati, and A. Masiero, Phys.Rev.Lett.57:961(1986).

[11] C.L. Bennett et al., [WMAP Collaboration]
*Astrophys.J.Suppl.*148:1(2003), [arXiv:astro-ph/0302207].
 D.N. Spergel et al., [WMAP Collaboration]
*Astrophys.J.Suppl.*148:175(2003), [arXiv:astro-ph/0302209].

[12] J.R. Ellis, K.A. Olive, Y. Santoso and V.C. Spanos, *Phys.Lett.B*565:176(2003), [arXiv:hep-ph/0303043].

[13] M. Battaglia, A. De Roeck, J.R. Ellis, F. Gianotti, K.A. Olive, and L. Pape, [arXiv:hep-ph/0306219].

[14] J.R. Ellis, K.A. Olive, Y. Santoso and V.C. Spanos, [arXiv:hep-ph/0310356].
 H. Baer and C. Balazs, *JCAP* 0305 (2003) 006, [arXiv:hep-ph/0303114].
 H. Baer, C. Balazs, A. Belyaev, T. Krupovnickas, X. Tata *JHEP* 0306 (2003) 054 [arXiv:hep-ph/0304303].
 A.B. Lahanas and D.V. Nanopoulos, *Phys.Lett.B*568:55(2003), [arXiv:hep-ph/0303130].
 U. Chattopadhyay, A. Corsetti, and P. Nath, *Phys.Rev.D*68:035005(2003), [arXiv:hep-ph/0303201].
 R. Arnowitt, B. Dutta, and B. Hu, [arXiv:hep-ph/0310103].

[15] J. Hisano, T. Moroi, K. Tobe, M. Yamaguchi and T. Yanagida, *Phys.Lett.B*357:579(1995), [arXiv:hep-ph/9501407].

[16] J. Hisano, T. Moroi, K. Tobe and M. Yamaguchi, *Phys.Rev.D*53:2442(1996), [arXiv:hep-ph/9510309].

[17] J. A. Casas and A. Ibarra, *Nucl.Phys.B*618:171(2001), [arXiv:hep-ph/0103065].

[18] J. Hisano, D. Nomura *Phys.Rev. D*59 (1999) 116005 [arXiv:hep-ph/9810479].
 W. Buchmuller, D. Delepine and F. Vissani, *Phys.Lett.B*459:171(1999), [arXiv:hep-ph/9904219].
 M.E. Gomez, G.K Leontaris, S. Lola, and J.D. Vergados, *Phys.Rev.D*59:116009(1999), [arXiv:hep-ph/9810251].

J.R. Ellis, M.E. Gomez, G.K. Leontaris, S. Lola, and D.V. Nanopoulos, Eur.Phys.J.C14:319(2000), [arXiv:hep-ph/9911459].

W. Buchmuller, D. Delepine and L.T. Handoko, Nucl.Phys.B576:445(2000), [arXiv:hep-ph/9912317].

J.L. Feng, Y. Nir, and Y. Shadmi, Phys.Rev.D61:113005(2000), [arXiv:hep-ph/9911370].

T. Blazek and S.F. King Phys.Lett.B518:109(2001), [arXiv:hep-ph/0105005].

D. Carvalho, J. Ellis, M. Gomez, and S. Lola, Phys.Lett.B515:323(2001), [arXiv:hep-ph/0103256].

S. Lavignac, I. Masina, and C.A. Savoy, Phys.Lett.B520:269(2001), [arXiv:hep-ph/0106245].

S. Lavignac, I. Masina, and C.A. Savoy, Nucl.Phys.B633:139(2002), [arXiv:hep-ph/0202086].

F. Deppisch, H. Pas, A. Redelbach, R. Ruckl, and Y. Shimizu, [arXiv:hep-ph/0206112].

J. Ellis, J. Hisano, M. Raidal, and Y. Shimizu, [arXiv:hep-ph/0206110].

[19] M.L. Brooks et.al., [MEGA Collaboration] Phys.Rev.Lett.83:1521(1999), [arXiv:hep-ph/9905013].

[20] T. Mori, “Status and Future of $\mu \rightarrow e\gamma$: The PSI Experiment,” Nucl. Phys. Proc. Suppl. 111, 194 (2002). Also, the MEG website <http://meg.web.psi.ch/>.

[21] U. Bellgardt et. al., Nucl.Phys.B229:1(1988),

[22] P. Wintz, “Results of the SINDRUM-II Experiment,” *Prepared for 29th International Conference on High-Energy Physics (ICHEP 98), Vancouver, Canada, 23-29 Jul 1998*

[23] M. Hebert [MECO Collaboration], “Searching for Muon to Electron Conversion Below the 10^{-16} Level,” Nucl. Phys. A 721, 461 (2003). Also, the MECO website <http://meco.ps.uci.edu/>.

[24] A. Sato: presentation at NuFact03
<http://www.cap.bnl.gov/nufact03/WG2/6june/sato.pdf>

[25] Y. Kuno and Y. Okada, Rev.Mod.Phys.73:151(2001), [arXiv:hep-ph/9909265].

7 Appendix

7.1 $l_j^- \rightarrow l_i^- \gamma$

The on-shell amplitude for $l_j^- \rightarrow l_i^- \gamma$ is given by,

$$T = e\epsilon^\alpha \bar{u}_i(p - q) \left(m_{l_j} i\sigma_{\alpha\beta} q^\beta (A_2^L P_L + A_2^R P_R) \right) u_j(p). \quad (22)$$

In the above, ϵ is the photon polarization vector and $A_2^{L,R}$ are the dipole coefficients. The decay rate for $\mu \rightarrow e\gamma$ can be expressed using eq.(22) as,

$$\Gamma(\mu \rightarrow e\gamma) = \frac{e^2}{16\pi} m_\mu^5 (|A_2^L|^2 + |A_2^R|^2). \quad (23)$$

Each dipole coefficient can be broken up into the sum of two terms,

$$A_2^{L,R} = A_2^{(n)L,R} + A_2^{(c)L,R}, \quad (24)$$

where (c) and (n) refer to the chargino and neutralino loop contributions. The expressions [15] for these contributions are,

$$\begin{aligned} A_2^{(n)L} &= \frac{1}{32\pi^2} \frac{1}{m_{\tilde{l}_X}^2} \left[N_{iAX}^{L(l)} N_{jAX}^{L(l)*} \frac{1}{6(1-r_n)^4} \right. \\ &\quad \times (1 - 6r_n + 3r_n^2 + 2r_n^3 - 6r_n^2 \ln r_n) \\ &\quad \left. + N_{iAX}^{L(l)} N_{jAX}^{R(l)*} \frac{M_{\tilde{\chi}_A^0}}{m_{l_j}} \frac{1}{(1-r_n)^3} (1 - r_n^2 + 2r_n \ln r_n) \right] \end{aligned} \quad (25)$$

$$A_2^{(n)R} = A_2^{(n)L}|_{L \leftrightarrow R}, \quad (26)$$

$$\begin{aligned} A_2^{(c)L} &= -\frac{1}{32\pi^2} \frac{1}{m_{\tilde{\nu}_X}^2} \left[C_{iAX}^{L(l)} C_{jAX}^{L(l)*} \frac{1}{6(1-r_c)^4} \right. \\ &\quad \times (2 + 3r_c - 6r_c^2 + r_c^3 + 6r_c \ln r_c) \\ &\quad \left. + C_{iAX}^{L(l)*} C_{jAX}^{R(l)*} \frac{M_{\tilde{\chi}_A^-}}{m_{l_j}} \frac{1}{(1-r_c)^3} (-3 + 4r_c - r_c^2 - 2 \ln r_c) \right] \end{aligned} \quad (27)$$

$$A_2^{(c)R} = A_2^{(c)L}|_{L \leftrightarrow R}, \quad (28)$$

where $r_n = M_{\tilde{\chi}_A^0}/m_{\tilde{l}_X}^2$ and $r_c = M_{\tilde{\chi}_A^-}/m_{\tilde{\nu}_X}^2$, and

$$C_{iAX}^R = -g_2(O_R)_{A1}U_{X,i}^\nu \quad (29)$$

$$C_{iAX}^L = g_2 \frac{m_{l_i}}{\sqrt{2}m_W \cos \beta} (O_L)_{A2}U_{X,i}^\nu, \quad (30)$$

$$N_{iAX}^{R(l)} = -\frac{g_2}{\sqrt{2}} \left([-(O_N)_{A2} - (O_N)_{A1} \tan \theta_W] U_{X,i}^l + \frac{m_{l_i}}{m_W \cos \beta} (O_N)_{A3} U_{X,i+3}^l \right) \quad (31)$$

$$N_{iAX}^{L(l)} = -\frac{g_2}{\sqrt{2}} \left(\frac{m_{l_i}}{m_W \cos \beta} (O_N)_{A3} U_{X,i}^l + 2(O_N)_{A1} \tan \theta_W U_{X,i+3}^l \right). \quad (32)$$

The matrices in the above expressions are defined in [15].

7.2 Renormalization Group Equations

For energy scales above the Majorana scale \mathcal{M} , the seesaw sector propagates unsuppressed.

Using the notation, $d\mathbf{X}/d \ln Q = \dot{\mathbf{X}}/16\pi^2$, the beta functions of the seesaw sectors are:

$$\dot{\mathbf{Y}}_\nu = \mathbf{Y}_\nu \left(-g_Y^2 \mathbf{I} - 3g_2^2 \mathbf{I} + 3\text{Tr}(\mathbf{Y}_u^\dagger \mathbf{Y}_u) \mathbf{I} + \text{Tr}(\mathbf{Y}_\nu^\dagger \mathbf{Y}_\nu) \mathbf{I} + 3\mathbf{Y}_\nu^\dagger \mathbf{Y}_\nu + \mathbf{Y}_e^\dagger \mathbf{Y}_e \right) \quad (33)$$

$$\dot{\mathbf{m}}_\nu^2 = 2\mathbf{m}_\nu^2 \mathbf{Y}_\nu \mathbf{Y}_\nu^\dagger + 2\mathbf{Y}_\nu \mathbf{Y}_\nu^\dagger \mathbf{m}_\nu^2 + 4\mathbf{Y}_\nu \mathbf{m}_L^2 \mathbf{Y}_\nu^\dagger + 4m_{H_u}^2 \mathbf{Y}_\nu \mathbf{Y}_\nu^\dagger + 4\mathbf{A}_\nu \mathbf{A}_\nu^\dagger \quad (34)$$

$$\begin{aligned} \dot{\mathbf{A}}_\nu = & -g_Y^2 \mathbf{A}_\nu - 3g_2^2 \mathbf{A}_\nu + 3\text{Tr}(\mathbf{Y}_u^\dagger \mathbf{Y}_u) \mathbf{A}_\nu + \text{Tr}(\mathbf{Y}_\nu^\dagger \mathbf{Y}_\nu) \mathbf{A}_\nu \\ & - 2g_Y^2 M_1 \mathbf{Y}_\nu - 6g_2^2 M_2 \mathbf{Y}_\nu + 6\text{Tr}(\mathbf{Y}_u^\dagger \mathbf{A}_u) \mathbf{Y}_\nu + 2\text{Tr}(\mathbf{Y}_\nu^\dagger \mathbf{A}_\nu) \mathbf{Y}_\nu \\ & + 4\mathbf{Y}_\nu \mathbf{Y}_\nu^\dagger \mathbf{A}_\nu + 5\mathbf{A}_\nu \mathbf{Y}_\nu^\dagger \mathbf{Y}_\nu + 2\mathbf{Y}_\nu \mathbf{Y}_e^\dagger \mathbf{A}_e + \mathbf{A}_\nu \mathbf{Y}_e^\dagger \mathbf{Y}_e \end{aligned} \quad (35)$$

While above the Majorana scale, the beta functions of the CMSSM couplings and masses are augmented by the seesaw sector.

$$\Delta \dot{\mathbf{Y}}_e = \mathbf{Y}_e \mathbf{Y}_\nu^\dagger \mathbf{Y}_\nu \quad (36)$$

$$\Delta \dot{m}_{H_u}^2 = 2\text{Tr}(\mathbf{m}_L^2 \mathbf{Y}_\nu^\dagger \mathbf{Y}_\nu + \mathbf{Y}_\nu^\dagger \mathbf{m}_\nu^2 \mathbf{Y}_\nu + m_{H_u}^2 \mathbf{Y}_\nu^\dagger \mathbf{Y}_\nu + \mathbf{A}_\nu^\dagger \mathbf{A}_\nu) \quad (37)$$

$$\Delta \dot{\mathbf{m}}_{\tilde{L}}^2 = \mathbf{m}_{\tilde{L}}^2 \mathbf{Y}_\nu^\dagger \mathbf{Y}_\nu + \mathbf{Y}_\nu^\dagger \mathbf{Y}_\nu \mathbf{m}_{\tilde{L}}^2 \quad (38)$$

$$+ 2 \mathbf{Y}_\nu^\dagger \mathbf{m}_\nu^2 \mathbf{Y}_\nu + 2 m_{H_u}^2 \mathbf{Y}_\nu^\dagger \mathbf{Y}_\nu + 2 \mathbf{A}_\nu^\dagger \mathbf{A}_\nu \quad (39)$$

$$\Delta \dot{\mathbf{A}}_e = \mathbf{Y}_e \mathbf{Y}_\nu^\dagger \mathbf{A}_\nu + \mathbf{A}_e \mathbf{Y}_\nu^\dagger \mathbf{Y}_\nu \quad (40)$$

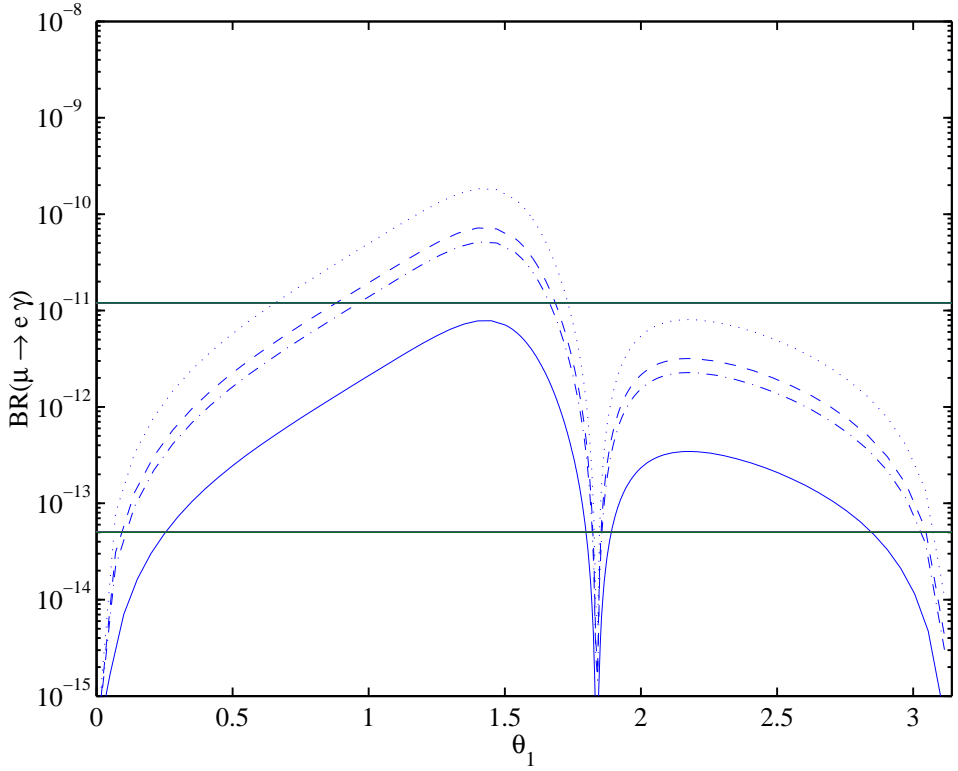


Figure 1: **Hierarchical ν_R s:** $\text{BR}(\mu \rightarrow e\gamma)$ as a function of the seesaw parameter θ_1 ; $\mu > 0$ and $a = 0$. The solid curve corresponds to $\tan \beta = 5$, $m_0 = 140$ GeV, $m_{1/2} = 700$ GeV. The dash-dot curve corresponds to $\tan \beta = 10$, $m_0 = 125$ GeV, $m_{1/2} = 560$ GeV. The dashed curve corresponds to $\tan \beta = 20$, $m_0 = 200$ GeV, $m_{1/2} = 760$ GeV. The dotted curve corresponds to $\tan \beta = 40$, $m_0 = 390$ GeV, $m_{1/2} = 900$ GeV. Each parameter set is chosen to lie inside the CMSSM allowed region [12]. The upper horizontal line indicates the present experimental bound and the lower line indicates the expected upcoming experimental sensitivity from MEG.

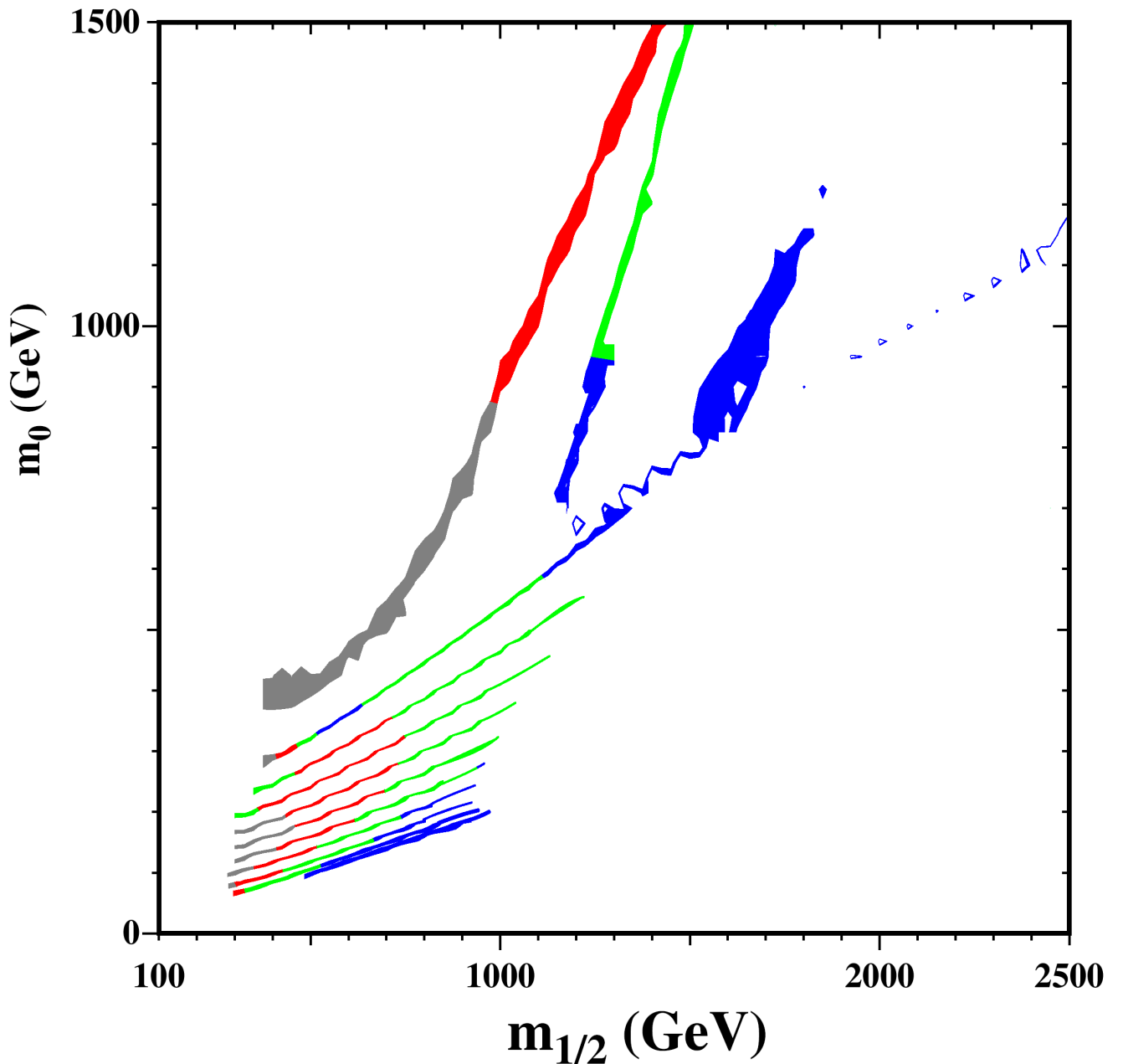


Figure 2: **Hierarchical ν_R s:** WMAP and laboratory constraint parameterization of the CMSSM, and LFV compliance, based on the current LFV bound, $\text{BR}(\mu \rightarrow e\gamma) < 1.2 \times 10^{-11}$ for $\tan \beta = 5, 10, 15, 20, 25, 30, 35, 40, 45, 50, 55$, $\mu > 0$ and $a = 0$. Grey indicates that less than 25% of the range of θ_1 is allowed. Red indicates that between 25% and 50% of θ_1 is allowed. Green and blue illustrate that 50% to 75%, and 75% to 100%, are allowed respectively. The constraint regions are reproduced from [12].

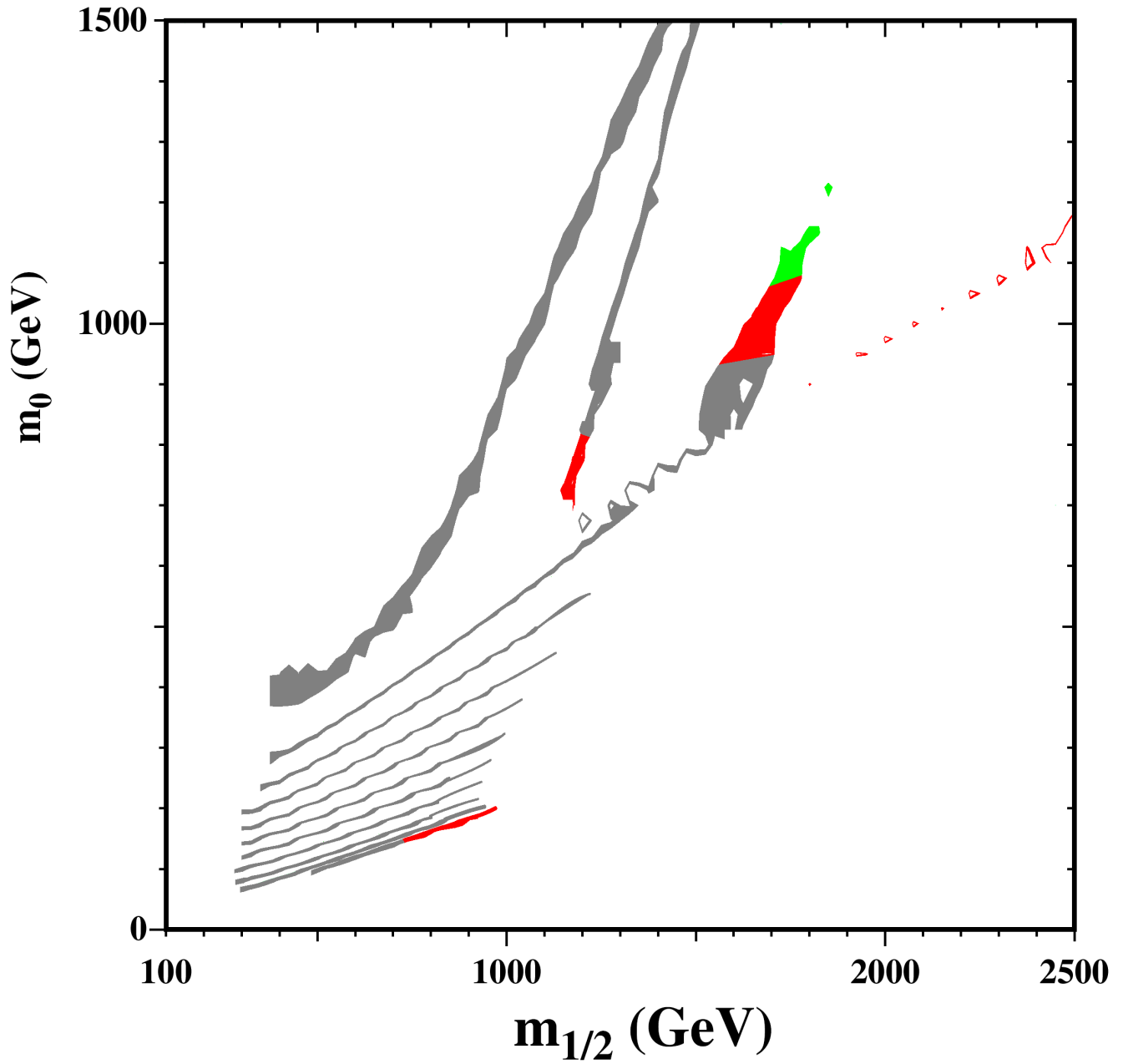


Figure 3: **Hierarchical ν_R s:** WMAP and laboratory constraint parameterization of the CMSSM, and LFV compliance, based on the expected LFV bound from MEG, $\text{BR}(\mu \rightarrow e\gamma) \lesssim 5 \times 10^{-14}$ for $\tan \beta = 5, 10, 15, 20, 25, 30, 35, 40, 45, 50, 55$, $\mu > 0$ and $a = 0$. Grey indicates that less than 25% of the range of θ_1 is allowed. Red indicates that between 25% and 50% of θ_1 is allowed. Green and blue illustrate that 50% to 75%, and 75% to 100%, are allowed respectively. The constraint regions are reproduced from [12].

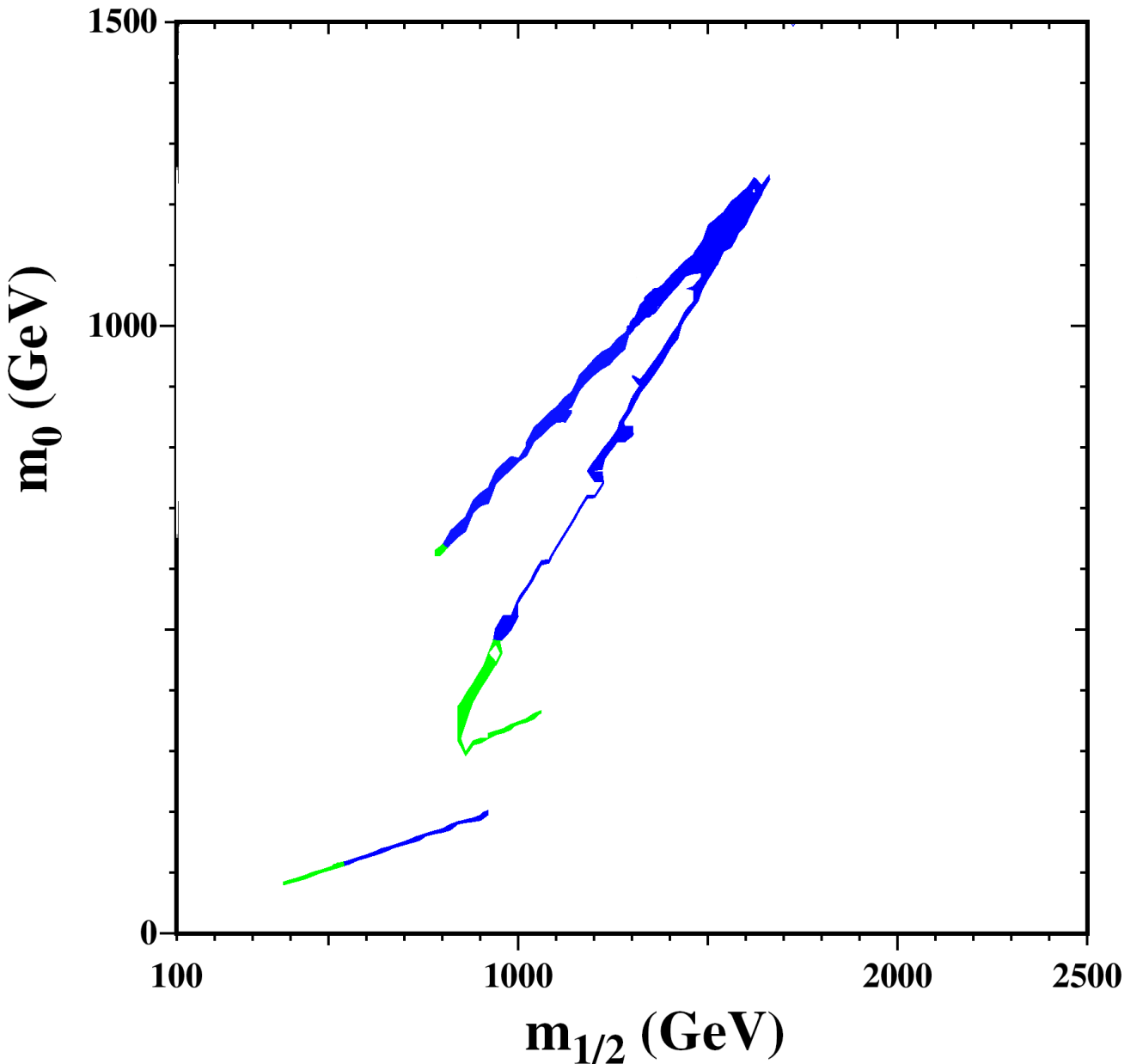


Figure 4: **Hierarchical ν_R s:** WMAP and laboratory constraint parameterization of the CMSSM, and LFV compliance, based on the current LFV bound, $\text{BR}(\mu \rightarrow e\gamma) < 1.2 \times 10^{-11}$ for $\tan \beta = 10, 35$, $\mu < 0$ and $a = 0$. Grey indicates that less than 25% of the range of θ_1 is allowed. Red indicates that between 25% and 50% of θ_1 is allowed. Green and blue illustrate that 50% to 75%, and 75% to 100%, are allowed respectively. The constraint regions are reproduced from [13].

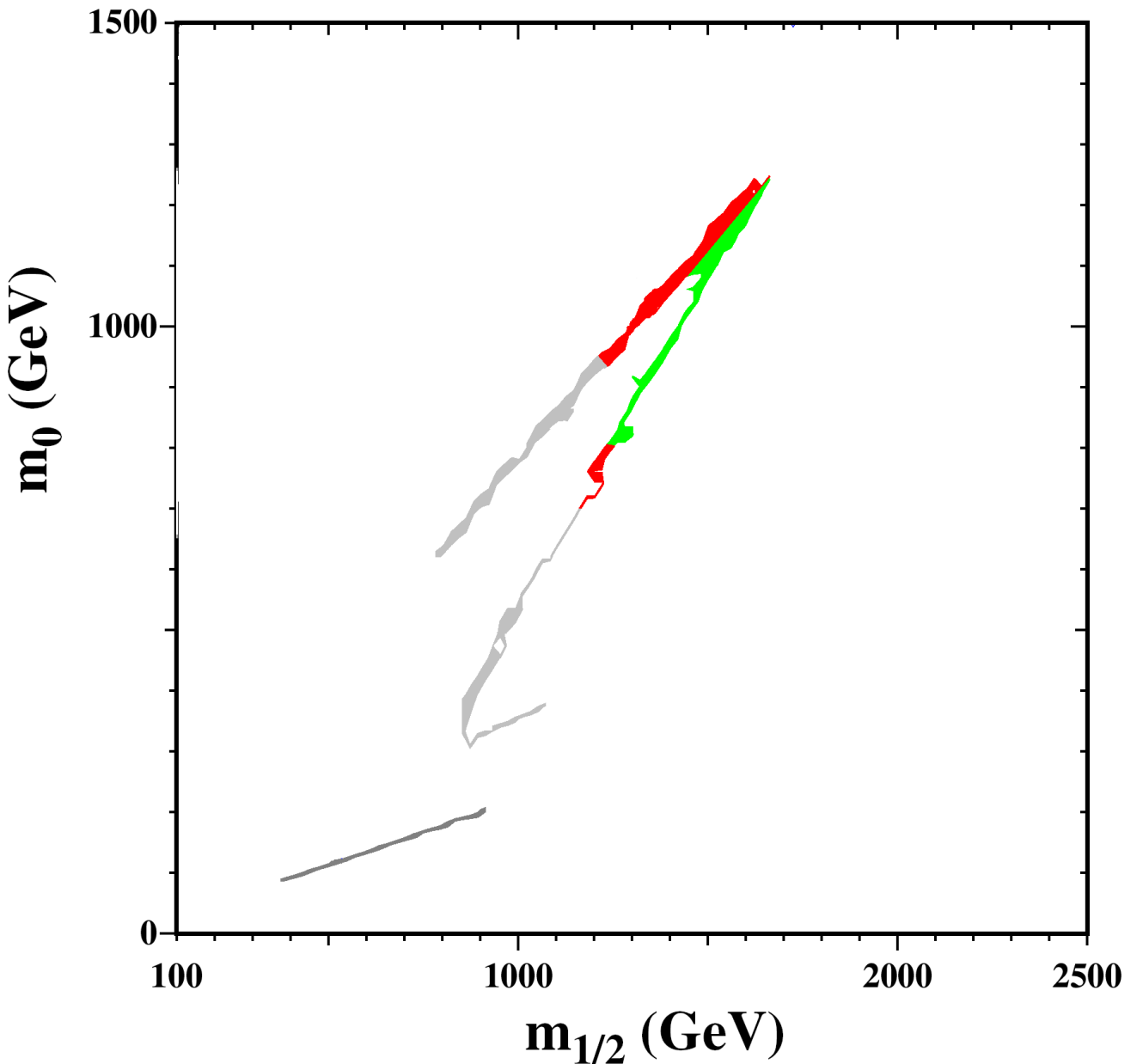


Figure 5: **Hierarchical ν_R s:** WMAP and laboratory constraint parameterization of the CMSSM, and LFV compliance, based on the expected LFV bound from MEG, $\text{BR}(\mu \rightarrow e\gamma) \lesssim 5 \times 10^{-14}$ for $\tan \beta = 10, 35$, $\mu < 0$ and $a = 0$. Grey indicates that less than 25% of the range of θ_1 is allowed. Red indicates that between 25% and 50% of θ_1 is allowed. Green and blue illustrate that 50% to 75% and 75% to 100% are allowed respectively.

The constraint regions are reproduced from [13].

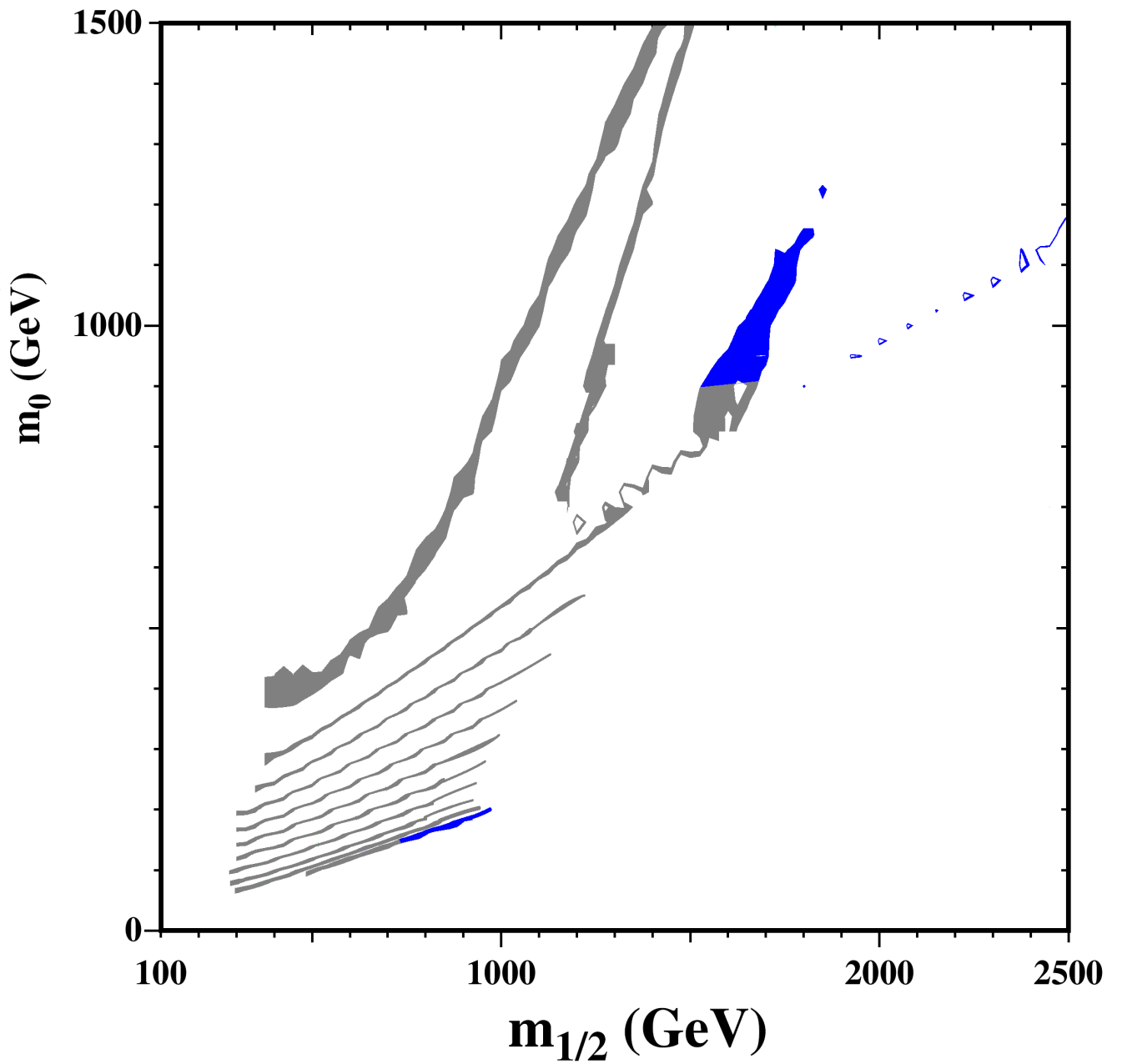


Figure 6: **Degenerate ν_R s:** WMAP and laboratory constraint parameterization of the CMSSM, and LFV compliance, based on the current LFV bound, $\text{BR}(\mu \rightarrow e\gamma) < 1.2 \times 10^{-11}$ for $\tan \beta = 5, 10, 15, 20, 25, 30, 35, 40, 45, 50, 55$, $\mu > 0$ and $a = 0$. Blue indicates the allowed region. The constraint regions are reproduced from [12].

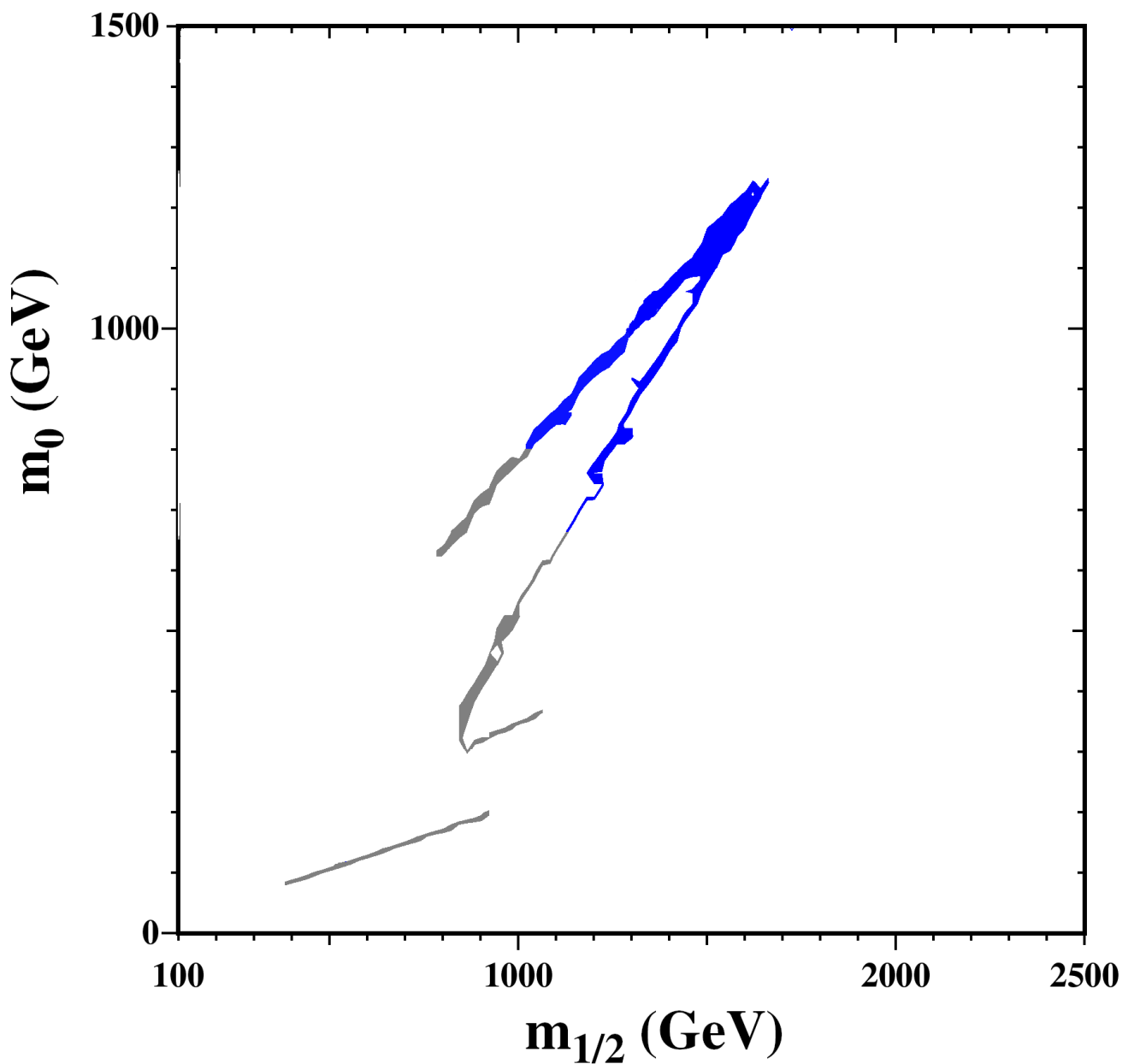


Figure 7: **Degenerate ν_R s:** WMAP and laboratory constraint parameterization of the CMSSM, and LFV compliance, based on the current LFV bound, $\text{BR}(\mu \rightarrow e\gamma) < 1.2 \times 10^{-11}$ for $\tan \beta = 10, 35$, $\mu < 0$ and $a = 0$. Blue indicates the allowed region. The constraint regions are reproduced from [13].